Accepted Manuscript

A facile approach to prepare phosphorus and nitrogen containing macromolecular covalent organic nanosheets for enhancing flame retardancy and mechanical property of epoxy resin

Xiaowei Mu, Dong Wang, Ying Pan, Wei Cai, Lei Song, Yuan Hu

PII: S1359-8368(18)30921-1

DOI: https://doi.org/10.1016/j.compositesb.2018.12.036

Reference: JCOMB 6365

To appear in: *Composites Part B*

Received Date: 21 March 2018

Revised Date: 31 October 2018

Accepted Date: 11 December 2018

Please cite this article as: Mu X, Wang D, Pan Y, Cai W, Song L, Hu Y, A facile approach to prepare phosphorus and nitrogen containing macromolecular covalent organic nanosheets for enhancing flame retardancy and mechanical property of epoxy resin, *Composites Part B* (2019), doi: https://doi.org/10.1016/j.compositesb.2018.12.036.

A facile approach to prepare phosphorus and nitrogen containing macromolecular covalent organic nanosheets for enhancing flame retardancy and mechanical property of epoxy resin

Xiaowei Mu[1], Dong Wang[2], Ying Pan[3], Wei Cai[1], Lei Song*[1], Yuan Hu*[1]

1 State Key Laboratory of Fire Science, University of Science and Technology of China, Hefei 230026, China

2 Key Laboratory of Eco-Textile, Ministry of Education, Jiangnan University, 1800 Lihu Road, Wuxi, 214122, China

3 Institute of Environmental Materials and Applications, College of Materials and Environmental Engineering, Hangzhou Dianzi University, 310018 Hangzhou, China

* Correspondence to: Yuan Hu; Lei Song.

Tel/fax: +86-551-63601664

E-mail: yuanhu@ustc.edu.cn; leisong@ustc.edu.cn

Abstract

The novel phosphorus and nitrogen containing covalent organic frameworks nanosheets, DOPO-COFs nanosheets have been synthesized through one step and then incorporated into epoxy resin (EP) by in situ polymerization. The successful preparation of DOPO-COFs nanosheets have been proved by vanishment of P-H group in FTIR curve of DOPO-COFs nanosheets, nano-size sheet with a lateral size of several micrometers in TEM image, and present of nitrogen and phosphorus elements in EDS pattern. The DOPO-COFs nanosheets show good dispersibility in EP matrix. The well-dispersed DOPO-COFs nanosheets contribute to thermal, mechanical, and flame retardant performances of EP. The weight loss rate of EP/3.2 wt% DOPO-COFs nanosheets decreases by 29.4 %. The storage modulus (30 ^{o}C) and fracture strength of EP 4 increases by 64.5 % and 15.6 % compared with that of untreated one, respectively. The PHRR and THR of EP loaded with 3.2 wt% of DOPO-COFs nanosheets decrease by 18.4 % and 18.5%, respectively. The feasible mode of action for inhibiting fire hazard of EP nanocomposites has also been put forward.

Key words: DOPO-COFs nanosheets, flame retardancy, mechanical performance, pyrolysis, fire hazard.

1 Introduction

Since the difficulty that organic frameworks with high crystallinity are hard to achieve has been conquered in 2005 [1, 2], covalent organic frameworks (COFs) have become one of the most concerned research areas after graphene due to their intrinsic micro or mesoporous chemical structure. COFs are two-dimensional or

three-dimensional crystalline organic porous substances connected by strong covalent bonds [3-5]. The reports of preparation of new COFs increase year by year since 2005. Now, researchers around the world pay more and more attention to preparation of functional COFs materials and synthesis of two-dimensional or one-dimensional COFs derivatives including COFs nanosheets and COFs hollow spheres.

Dozens of COFs composited by different reagents have been synthesized [6, 7]. Functional COFs and their derivatives have already been applied into every walk of life including gas storage and separation [8, 9], catalysis [5, 10, 11], chemical sensors [12], electrochemical and clean energy [13-17], and nano channels [18]. It is reported that pyrolytic graphite [19], flat faces of Au made on homemade single-crystal beads [20], graphene [7] and hexagonal boron nitride [12] can work as a template, resulting in preparation of COFs nanosheets with several atomic thick. Monolayer COFs nanosheets can also been prepared at the air/water [21] and solid/vapor interface [22]. COFs nanosheets with several layers have also been synthesized by ultrasound or mechanical ball milling. COF-8 prepared from condensation reaction between 2,3,6,7,10,11-hexahydroxytriphenylene and 1,3,5-tris[4-phenylboronic acid]benzene is exfoliated into nanosheets in dichloromethane under sonication [23]. The effect of sonication conditions and structure characteristics on the lateral dimensions, thickness, and quality of exfoliated COFs nanosheets has also been studied [15]. High thermal-stable COFs nanosheets prepared from condensation reaction between triformylphloroglucinol and diamine-containing substances have been achieved from their bulk COFs through ball milling [24, 25]. Hollow micro/nanospheres have also

been prepared without any template [26]. However, the method of preparing COFs nanosheets above are usually low yield and strict. Besides, raw materials used to synthesize COFs nanosheets are expensive. Thus, it is important to preparation of COFs nanosheets through an efficient and convenient method. COFs prepared from condensation reaction between melamine and o-phthalaldehyde (OPA) are synthesized cheaply and exfoliated easily into nanosheets in our group [27], which provides an opportunity to broaden application of COFs into polymer matrix.

Epoxy resin (EP), as one of the most widespread applied polymer, has been applied in electronic and electrical industry, surface coatings, and adhesives, etc. due to its good performances [28, 29]. However, conventional EP is flammable, which seriously limits its application in many areas. Thus, a large number of flame retardants have been synthesized and applied into EP [30, 31]. 9,10-dihydro-9-oxa-10-phosphaphenanthrene-10-oxide (DOPO)，an one of the most efficient flame retardants for EP, has been widely applied to retard combustion of EP. However, deterioration of mechanical performances occurs due to decreased cross-linking density of EP resulted from incorporating of DOPO. In this study, COFs nanosheets are first reacted with DOPO and then incorporated into EP through in situ polymerization. The DOPO-COFs nanosheets not only function flame retardancy, but also have good effect on mechanical performance of EP. The thermal stability, flame retardancy, mechanical and CO suppression properties of EP nanocomposites have also been studied.

2 Experimental

2.1 Materials

EP (DGEBA, E-44) was provided by Hefei Jiangfeng Chemical Industry Co. Ltd. (China). Melamine, methanol, acetone, dimethyl sulfoxide (DMSO), acetic acid (98 wt%), N,N-Dimethylformamide (DMF), 4,4-Diaminodiphenyl methane (DDM), and tetrahydrofuran (THF) were purchased from Sinopharm Chemical Reagent Co., Ltd. (China). DOPO and OPA were obtained from Aladdin Chemistry Co., Ltd. (China).

2.2 Preparation of DOPO-COFs nanosheets

COFs nanosheets prepared from condensation reaction between melamine and OPA are prepared through ball milling [27]. COFs nanosheets (1 g) and DOPO (4.6 g) were dispersed in DMF and then the system was heated with stirring under nitrogen atmosphere at 120 ^{o}C for 18 h. The resultant DOPO-COFs nanosheets were achieved through filtration and then washing with DMF and THF in order. Finally, DOPO-COFs nanosheets were re-dispersed in THF under ultrasound.

2.3 Preparation of EP/DOPO-COFs nanosheets nanocomposite

DOPO-COFs nanosheets were dispersed in THF under ultrasound for 2 h and then the resultant suspension was mixed with EP at 80 ^{o}C for 10 h to remove THF. Finally, above system which was mixed with DDM was prepared into samples with different weight loading of DOPO-COFs nanosheets through first being heated at 100 ^{o}C for 2 h and then being heated at 150 ^{o}C for 2 h. The EP nanocomposites with 0, 0.4, 0.8, 1.6, and 3.2 wt% DOPO-COFs nanosheets are named as EP 0, EP 1, EP 2, EP 3, and EP 4, respectively. The EP nanocomposite loaded with 3.2 wt% COFs nanosheets is called as EP Control. The detailed preparation process is illuminated in Figure 1.

2.4 Characterization

Chemical groups of samples were characterized by Fourier transform infrared (FTIR) spectra measured on a Nicolet 6700 spectrometer (Nicolet Instrument Corp., US) with a wavenumber range of 4000 – 400 cm^{-1}. Thermogravimetric analysis (TGA) curves of samples with a mass range from 3 to 5 mg were investigated on a Q5000 thermoanalyzer instrument (TA Instruments Inc., US) with a linear heating rate of 20 $^{o}C\ min^{-1}$ from room temperature to 800 ^{o}C. X-ray photoelectron spectroscopy (XPS) was monitored on a VG ESCALAB 250 electron spectrometer (Thermo VG. Scientific Ltd., UK) with an Al Kα line (1486.6 eV). Transmission electron microscopy (TEM) tests were measured on a JEM-2100F microscope (JEOL Co., Ltd., Japan) with an acceleration voltage of 200 kV. The atomic force microscopy (AFM) image was performed in tapping mode through a DI Multimode V scanning probe microscope. Morphologies of fractured surface were shown on a FEI Sirion 200 scanning electron microscope (SEM) with an acceleration voltage of 5 kV (JEOL Co., Ltd., Japan) to investigate dispersion state of DOPO-COFs nanosheets. Dynamic mechanical analysis (DMA) was analyzed by a DMA Q800 instrument (TA Instruments Inc., USA) at a fixed frequency of 1 Hz from 25 ^{o}C to 220 ^{o}C. Fracture strength and yield strength of samples were conducted on a WD-20D electronic universal testing instrument (Changchun Intelligent Instrument Co., Ltd., China) at a crosshead speed of 2 mm min^{-1} according to the Chinese standard method (GB 13022-91). Combustion properties of samples were displayed on a cone calorimeter (Fire Testing Technology, UK) according to ISO 5660 standard under a 35 kW m^{-2}

heat flux. The limiting oxygen index (LOI) was measured on a C-2 oxygen index meter (Jiangning Analysis Instrument Co., Ltd, China) according to ASTM D2863-97 standard. UL-94 vertical burning test was conducted on a CZF-II horizontal and vertical burning tester (Jiangning Analysis Instrument Co., Ltd, China) on the basic of ASTM D3801 standard. The thermal degradation gaseous products were characterized by a TGA Q5000IR thermogravimetric analyzer, linked to a Nicolet 6700 FTIR spectrophotometer (TG/IR) from room temperature to 700 ^{o}C with a heating rate of 20 ^{o}C/min in helium atmosphere. A LABRAM-HR laser confocal Raman spectroscope (Jobin Yvon Co., Ltd, France) with a 514.5 nm argon laser line was applied to study the degree of graphitization of char residues of samples.

3 Results and discussions

3.1 Characterization of COFs and DOPO-COFs nanosheets.

The FTIR, TEM, XRD and EDS tests have been done to investigate chemical bonds, morphology and element constitute of samples. As shown in Figure 2 (a), the peaks of COFs at 3401, 1726, and 1350 cm^{-1} are assigned to stretching vibration of NH groups in aromatic ring, unreacted aldehyde group, and -NH- stretching vibration, respectively [32-34]. The successful incorporation of melamine into COFs is proved by two peaks centered at 1568 and 1469 cm^{-1}, which represent the quadrant and semicircle stretching of the s-triazine ring [35]. The peaks of COFs at 1209 and 810 cm^{-1} belong to aromatic stretching vibration of C-N bond. The peak in FTIR curve of DOPO centered at 3058 cm^{-1} is attributed to C-H stretching vibration of aromatic ring. The bonds at 1614, 1510 and 1471 cm^{-1} belong to vibration of benzene ring skeleton

[36]. The peak of DOPO centered at 2437 cm^{-1} corresponds to stretching vibration of P-H bond [37]. The presence of P=O (1143 cm^{-1}) and P-O-Ph (1117 cm^{-1}) bonds of DOPO is also testified in Figure 2 (a) [38]. It is obvious that bond of P-H group disappears in FTIR curve of DOPO-COFs nanosheets, indicating occurrence of reaction between DOPO and COFs nanosheets [28]. Besides, it is shown in FTIR curve of DOPO-COFs nanosheeets that the peaks centered at 1157 and 1093 cm^{-1} are P=O and P-O-Ph stretching vibrations of DOPO, respectively. In Figure 2 (b), the intensity of typical peak of DOPO-COFs nanosheets at around 23.5^{o} decreases compared with that of COFs, indicating that COFs is exfoliated. It is deduced from Figure 2 (c) that three-dimensional porous COFs are achieved. As shown in Figure 2 (d), two-dimensional DOPO-COFs nanosheets with a lateral size from several hundred nanometers to several micrometers are prepared successfully. The present of nitrogen and phosphorus element in energy dispersive spectrometer (EDS) of DOPO-COFs nanosheets also indicates that COFs nanosheets are modified by DOPO successfully.

The thickness and structure of DOPO-COFs nanosheets have been investigated further through AFM test. It is obvious that all of nano-material in Figure 3 (a) presents two-dimensional sheets. The thicknesses of exfoliated DOPO-COFs in Figure 3 (b) vary from 7 to 35 nm corresponding to DOPO-COFs nanosheets in Figure 3 (a). The three-dimensional image of DOPO-COFs nanosheets are displayed in Figure 3 (c), it is significant that the thickness of DOPO-COFs nanosheets is not consistent, which is same as the results in Figure 3 (b).

Atom composition and chemical bonds of DOPO-COFs nanosheets have been studied further in Figure 4 and related data of atom percent have been listed in Table 1. The nitrogen, oxygen, carbon and phosphorous atoms have been confirmed in wide XPS scanning spectrum of DOPO-COFs nanosheets. It is inferred from high-resolution XPS spectra of C_{1s} that the peaks at 284.5 eV, 285.1 eV, 286.2 eV, 287.3 eV and 280.0 eV are assigned to C-C, C-N/C-P, C-O-P, C=N, and C=O bonds, respectively [39, 40]. The peaks in N_{1s} high-resolution XPS spectra of DOPO-COFs nanosheets represent N=C (398.4 eV) and N-H (399.7 eV) [35]. The characteristic peak at 133.0 eV in P_{2p} high-resolution XPS spectra corresponds to P-C or P-O-C or P=O bond [41]. Thus, it is concluded that DOPO-COFs nanosheets are prepared.

3.2 Thermal stability of DOPO-COFs nanosheets and their EP nanocomposites.

TGA and DTG curves of DOPO-COFs nanosheets and EP nanocomposites under nitrogen atmosphere are shown in Figure 5 and detailed data are listed in Table 2. It is significant that COFs nanosheets degrade earlier than that of COFs, which may be the reason for pyrolysis of low molecular fragments caused by ball milling of COFs. However, thermal stability of COFs nanosheets increases sharply after modified by DOPO. The temperature at 5 wt% weight loss ($T_{5\ wt\%}$) of DOPO-COFs nanosheets increases by 101 ^{o}C from 199 to 301 ^{o}C compared with that of COFs nanosheets. Besides, the char residues of DOPO-COFs nanosheets increase by 46.1 % compared with that of COFs. It is also inferred from Figure 5 (b) that weigh loss rate of DOPO-COFs nanosheets is lower than that of COFs. Thus, DOPO-COFs nanosheets display good thermal stability. As shown in Figure 5 (c), it is obvious that weight loss

rate of EP/3.2 wt% DOPO-COFs nanosheets decreases by 29.4 % compared with that of neat EP, indicating incorporating of DOPO-COFs nanosheets into EP contributes to retardation of pyrolysis of EP. However, the $T_{5\ wt\%}$ of EP nanocomposite decreases slightly compared with that of untreated one due to thermal degradation of DOPO-COFs in advance. It is observed from TGA curve that incorporating of DOPO-COFs nanosheets has little influence on char forming of EP nanocomposite, which may be explained that DOPO functions flame inhibition in gaseous phase [42].

3.3 Fractured surface characteristic and mechanical performance of EP and its nanocomposites.

The dispersion state of DOPO-COFs nanosheets and fractured surface of EP nanocomposite are investigated through SEM tests. In Figure 6, the fractured surface of neat EP is smooth. It is obvious that fractured surface of EP 4 is rougher than that of untreated one. This is due to strong interfacial adhesion between DOPO-COFs nanosheets and EP matrix. Besides, there is almost no agglomeration of DOPO-COFs nanosheets found in fractured surface of EP 4 from SEM images. In another word, DOPO-COFs nanosheets disperse well in EP matrix. As shown in Figure 6, the EP Control also shows a rough fractured surface. However, in Figure 6 (e), there are a large number of chippings, which may be due to the aggregation of COFs nanosheets in EP matrix. To further characterize the distribution of DOPO-COFs nanosheets in EP matrix, TEM ultrathin section images of EP Control and EP 4 has also been done. As shown in Figure 7 (a), COFs nanosheets aggregate in EP matrix in a certain degree. However, no agglomeration of DOPO-COFs nanosheets occurs although at high

weight loading (3.2 wt%). This may be because COFs nanosheets show better compatibility in EP matrix after being modified by DOPO, leading to good dispersibility of DOPO-COFs nanosheets in EP matrix. Besides, the DOPO-COFs still maintain their nanosheets structure in EP matrix. This result is consistent with the results of SEM test.

Storage modulus and fracture strength of EP and its nanocomposite have been studied and related dynamic mechanical property and stress-strain curves of samples have been illuminated in Figure 8. It is significant that storage modulus and fracture strength of EP loaded with 3.2 wt% of DOPO-COFs nanosheets is enhanced sharply compared with that of neat one. The storage modulus (30 ^{o}C) and fracture strength of EP 4 increases by 64.5 % and 15.6 % compared with that of untreated one, respectively. This is because DOPO-COFs nanosheets display better compatibility and tighter interfacial adhesion in EP than that of COFs nanosheets.

3.4 Combustion performances of EP and its nanocomposites.

Combustion property, as one of the most important performances to evaluate fire hazards, has been investigated through cone calorimetry, LOI and UL-94 vertical burning tests. Heat release rate (HRR), and total heat release (THR) curves of EP and its nanocomposites have been shown in Figure 9 and the detailed data are listed in Table 3. The detailed data of LOI and UL-94 vertical burning tests are also listed in Table 3. As you can see, incorporating of DOPO-COFs nanosheets has little influence on enhancement of UL-94 vertical burning rating. All of the samples are no rating in UL-94 vertical burning test. However, the LOI value of EP nanocomposite increases

with enhanced weight loading of DOPO-COFs nanosheets. The LOI of EP 4 is 25 %. The peak heat release rate (PHRR) and THR of EP decrease obviously after incorporating of DOPO-COFs nanosheets. The PHRR and THR of EP loaded with 3.2 wt% of DOPO-COFs nanosheets decrease by 18.4 % and 18.5%, respectively. However, the PHRR and THR of EP Control are higher than that of EP 4, which means modifying COFs nanosheets with DOPO contributes better flame retardancy to EP. The PHRR and THR of EP 2 are lower than that of other samples, this may be the reason for operation error during cone calorimetry tests. The related digital images of samples after cone calorimetry tests are displayed in Figure 10. The amount of left char residues increases slightly with increased weight loading of DOPO-COFs nanosheets.

3.5 Flame retardant mode of action in condensed and gaseous phases.

To further study why flame retardancy of EP nanocomposite is enhanced obviously with only slightly increase of char residues ? Influence of incorporating DOPO-COFs nanosheets on release of gaseous pyrolysis products of EP during thermal degradation has been studied by TG/IR test. The FTIR spectra of EP and EP 4 at the maximum pyrolysis rate are displayed in Figure 11. There is no obvious difference between two FTIR spectra of EP and EP 4, indicating the same volatile components during pyrolysis. The characteristic absorption peaks at 3656, 2977, 2356, 2180, 1752, and 1512 cm^{-1} are ascribed to H_2O and/or phenol, hydrocarbons, CO_2, CO, carbonyl compounds, and aromatic compounds, respectively [43, 44].

To investigate the changes of release of volatile pyrolysis products further, the

absorbance of pyrolysis products for EP and EP 4 versus temperature is shown in Figure 12. The release of volatile components of EP 4 occurs at around 350 ^{o}C which is lower than that of neat one. This result is consistent with that of TGA result. The absorption intensity of total pyrolysis products, flammable products (carbonyl and aromatic compounds) and toxic gas (CO) resulted from thermal degradation of EP 4 is lower than that of EP 0, this may contribute to reduction of PHRR of EP 4. However, incorporating of DOPO-COFs nanosheets has little influence on absorption intensity of hydrocarbons during pyrolysis. The intensity of released CO_2 increases, this may be caused by decomposition of pyrolysis products.

Raman tests of EP and its nanocomposites have been conducted to study flame retardant mode of action in condensed phase. The Raman spectra of char residues of samples have been shown in Figure 13. The peak centered at around 1365 cm^{-1} belongs to D bond which is resulted from the vibration of sp^2-hybridized carbon atoms in graphite layer. The G bond at around 1595 cm^{-1} represents an E_{2g} mode of hexagonal graphite [45]. The graphitization degree of the residual char is evaluated by the integrated intensities of D to G bond (I_D/I_G). The I_D/I_G of EP Control is lower than that of untreated EP but higher than that of EP 4. It is explained that incorporating of DOPO-COFs nanosheets has better influence on enhancement of graphitization degree of residual char of EP than that of COFs nanosheets. The char with higher graphitization degree shows better thermal stability and char quality, leading to better physical barrier effect. Thus, release of gaseous pyrolysis products and PHRR of EP nanocomposite decrease.

The feasible mode of action for inhibiting fire hazard of EP nanocomposites is shown below. COFs nanosheets show better dispersibility and compatibility in EP after being modified by DOPO. In condensed phase, the well-dispersed DOPO-COFs nanosheets contribute to graphitization degree of char, resulting in reduction of PHRR and gaseous pyrolysis products including CO, carbonyl and aromatic compounds. Thus suppression of fire hazards of EP is achieved.

4 Conclusions

A novel phosphorus and nitrogen containing COFs nanosheets, DOPO-COFs nanosheets have been synthesized and applied as flame retardant for EP. Not only are combustion performances of EP increased, but also mechanical property of EP is enhanced. The gaseous pyrolysis products including CO, carbonyl and aromatic compounds are also decreased due to physical barrier effect. The successful preparation of DOPO-COFs nanosheets is proved by vanishment of P-H group in FTIR curve of DOPO-COFs nanosheets, nano-size sheets with a lateral size of several micrometers in TEM image, and present of nitrogen and phosphorus elements in EDS pattern. The thermal stability of COFs nanosheets is increased obviously. $T_{5\ wt\%}$ and char residues of DOPO-COFs nanosheets increase by 101 ^{o}C and 46.1 % compared with that of untreated one under nitrogen. The weight loss rate of EP/3.2 wt% DOPO-COFs nanosheets also decreases by 29.4 %. The storage modulus (30 ^{o}C) and fracture strength of EP 4 increases by 64.5 % and 15.6 % compared with that of untreated one, respectively. The PHRR and THR of EP loaded with 3.2 wt% of DOPO-COFs nanosheets decrease by 18.4 % and 18.5%, respectively. DOPO-COFs

nanosheets display better dispersibility and compatibility in EP compared with that of COFs nanosheets. The well-dispersed DOPO-COFs nanosheets contribute to graphitization degree of char, resulting in reduction of PHRR and release of gaseous pyrolysis products.

Supplementary material

TGA and DTG curves of EP and its nanocomposites under air atmosphere.

Acknowledgements

The work was financially supported by the National Basic Research Program of China (973 Program) (2014CB931804), National Natural Science Foundation of China (51473154) and Fundamental Research Funds for the Central Universities (WK2320000032).

References

[1] L.Y. Chen, L. Zhang, Z.J. Chen, H.J. Liu, R. Luque, Y.W. Li, A covalent organic framework-based route to the in situ encapsulation of metal nanoparticles in N-rich hollow carbon spheres, Chem. Sci. 7 (2016) 6015-6020.

[2] A.P. Cote, A.I. Benin, N.W. Ockwig, M. O'keeffe, A.J. Matzger, O.M. Yaghi, Porous, crystalline, covalent organic frameworks, Science 310 (2005) 1166-1170.

[3] R.W. Tilford, S.J. Mugavero, P.J. Pellechia, J.J. Lavigne, Tailoring microporosity in covalent organic frameworks, Adv. Mater. 20 (2008) 2741-2746.

[4] R.W. Tilford, W.R. Gemmill, H.-C. zur Loye, J.J. Lavigne, Facile synthesis of a highly crystalline, covalently linked porous boronate network, Chem. Mater. 18 (2006) 5296-5301.

[5] S.-Y. Ding, J. Gao, Q. Wang, Y. Zhang, W.-G. Song, C.-Y. Su, W. Wang, Construction of covalent organic framework for catalysis: Pd/COF-LZU1 in Suzuki–Miyaura coupling reaction, J. Am. Chem. Soc. 133 (2011) 19816-19822.

[6] U. Díaz, A. Corma, Ordered covalent organic frameworks, COFs and PAFs. From preparation to application, Coordin. Chem. Rev. 311 (2016) 85-124.

[7] J.W. Colson, A.R. Woll, A. Mukherjee, M.P. Levendorf, E.L. Spitler, V.B. Shields, M.G. Spencer, J. Park, W.R. Dichtel, Oriented 2D covalent organic framework thin films on single-layer graphene, Science 332 (2011) 228-231.

[8] H. Furukawa, O.M. Yaghi, Storage of hydrogen, methane, and carbon dioxide in highly porous covalent organic frameworks for clean energy applications, J. Am. Chem. Soc. 131 (2009) 8875-8883.

[9] N. Huang, X. Chen, R. Krishna, D. Jiang, Two‐Dimensional Covalent Organic Frameworks for Carbon Dioxide Capture through Channel‐Wall Functionalization, Angew. Chem. Int. Edit. 127 (2015) 3029-3033.

[10] L. Stegbauer, K. Schwinghammer, B.V. Lotsch, A hydrazone-based covalent organic framework for photocatalytic hydrogen production, Chem. Sci. 5 (2014) 2789-2793.

[11] D.B. Shinde, S. Kandambeth, P. Pachfule, R.R. Kumar, R. Banerjee, Bifunctional covalent organic frameworks with two dimensional organocatalytic micropores, Chem. Commun. 51 (2015) 310-313.

[12] B. Sun, J. Li, W.-L. Dong, M.-L. Wu, D. Wang, Selective Growth of Covalent Organic Framework Ultrathin Films on Hexagonal Boron Nitride, J. Phys. Chem. C

120 (2016) 14706-14711.

[13] C.R. DeBlase, K.E. Silberstein, T.-T. Truong, H.D. Abruña, W.R. Dichtel, β-Ketoenamine-linked covalent organic frameworks capable of pseudocapacitive energy storage, J. Am. Chem. Soc. 135 (2013) 16821-16824.

[14] F. Xu, S. Jin, H. Zhong, D. Wu, X. Yang, X. Chen, H. Wei, R. Fu, D. Jiang, Electrochemically active, crystalline, mesoporous covalent organic frameworks on carbon nanotubes for synergistic lithium-ion battery energy storage, Sci. Rep-UK 5 (2015).

[15] I. Berlanga, R. Mas-Ballesté, F. Zamora, Tuning delamination of layered covalent organic frameworks through structural design, Chem. Commun. 48 (2012) 7976-7978.

[16] E.L. Spitler, W.R. Dichtel, Lewis acid-catalysed formation of two-dimensional phthalocyanine covalent organic frameworks, Nat. Chem. 2 (2010) 672-677.

[17] X. Ding, J. Guo, X. Feng, Y. Honsho, J. Guo, S. Seki, P. Maitarad, A. Saeki, S. Nagase, D. Jiang, Synthesis of metallophthalocyanine covalent organic frameworks that exhibit high carrier mobility and photoconductivity, Angew. Chem. Int. Edit. 50 (2011) 1289-1293.

[18] E.L. Spitler, M.R. Giovino, S.L. White, W.R. Dichtel, A mechanistic study of Lewis acid-catalyzed covalent organic framework formation, Chem. Sci. 2 (2011) 1588-1593.

[19] X.H. Liu, Y.P. Mo, J.Y. Yue, Q.N. Zheng, H.J. Yan, D. Wang, L.J. Wan, Isomeric Routes to Schiff‐Base Single‐layered Covalent Organic Frameworks, Small 10

(2014) 4934-4939.

[20] R. Tanoue, R. Higuchi, N. Enoki, Y. Miyasato, S. Uemura, N. Kimizuka, A.Z. Stieg, J.K. Gimzewski, M. Kunitake, Thermodynamically controlled self-assembly of covalent nanoarchitectures in aqueous solution, ACS Nano 5 (2011) 3923-3929.

[21] T.-Y. Zhou, Q.-Y. Qi, Q.-L. Zhao, J. Fu, Y. Liu, Z. Ma, X. Zhao, Highly thermally stable hydrogels derived from monolayered two-dimensional supramolecular polymers, Polym. Chem-UK 6 (2015) 3018-3023.

[22] X.-H. Liu, C.-Z. Guan, S.-Y. Ding, W. Wang, H.-J. Yan, D. Wang, L.-J. Wan, On-surface synthesis of single-layered two-dimensional covalent organic frameworks via solid–vapor interface reactions, J. Am. Chem. Soc. 135 (2013) 10470-10474.

[23] I. Berlanga, M.L. Ruiz‐González, J.M. González‐Calbet, J.L.G. Fierro, R. Mas‐Ballesté, F. Zamora, Delamination of layered covalent organic frameworks, Small 7 (2011) 1207-1211.

[24] S. Chandra, S. Kandambeth, B.P. Biswal, B. Lukose, S.M. Kunjir, M. Chaudhary, R. Babarao, T. Heine, R. Banerjee, Chemically stable multilayered covalent organic nanosheets from covalent organic frameworks via mechanical delamination, J. Am. Chem. Soc. 135 (2013) 17853-17861.

[25] Z. Kang, Y. Peng, Y. Qian, D. Yuan, M.A. Addicoat, T. Heine, Z. Hu, L. Tee, Z. Guo, D. Zhao, Mixed matrix membranes (MMMs) comprising exfoliated 2D covalent organic frameworks (COFs) for efficient CO_2 separation, Chem. Mater. 28 (2016) 1277-1285.

[26] T.-Y. Zhou, F. Lin, Z.-T. Li, X. Zhao, Single-step solution-phase synthesis of

free-standing two-dimensional polymers and their evolution into hollow spheres, Macromolecules 46 (2013) 7745-7752.

[27] X. Mu, J. Zhan, X. Feng, B. Yuan, S. Qiu, L. Song, Y. Hu, Novel Melamine/o-Phthalaldehyde Covalent Organic Frameworks Nanosheets: Enhancement Flame Retardant and Mechanical Performances of Thermoplastic Polyurethanes, ACS Appl. Mater. Inter. 9 (2017) 23017-23026.

[28] L. Gu, G. Chen, Y. Yao, Two novel phosphorus–nitrogen-containing halogen-free flame retardants of high performance for epoxy resin, Polym. Degrad. Stabi. 108 (2014) 68-75.

[29] G.-R. Xu, M.-J. Xu, B. Li, Synthesis and characterization of a novel epoxy resin based on cyclotriphosphazene and its thermal degradation and flammability performance, Polym. Degrad. Stabi. 109 (2014) 240-248.

[30] M.-J. Xu, G.-R. Xu, Y. Leng, B. Li, Synthesis of a novel flame retardant based on cyclotriphosphazene and DOPO groups and its application in epoxy resins, Polym. Degrad. Stabi. 123 (2016) 105-114.

[31] L. Qian, Y. Qiu, N. Sun, M. Xu, G. Xu, F. Xin, Y. Chen, Pyrolysis route of a novel flame retardant constructed by phosphaphenanthrene and triazine-trione groups and its flame-retardant effect on epoxy resin, Polym. Degrad. Stabi. 107 (2014) 98-105.

[32] Y. Yao, N. Ning, L. Zhang, T. Nishi, M. Tian, Largely improved electromechanical properties of thermoplastic polyurethane dielectric elastomer by carbon nanospheres, RSC Adv. 5 (2015) 23719-23726.

[33] M. Tian, B. Yan, Y. Yao, L. Zhang, T. Nishi, N. Ning, Largely improved actuation strain at low electric field of dielectric elastomer by combining disrupting hydrogen bonds with ionic conductivity, J. Mater. Chem. C 2 (2014) 8388-8397.

[34] Y. Ti, Q. Wen, D. Chen, Characterization of the hydrogen bond in polyurethane/attapulgite nanocomposites, J. Appl. Polym. Sci. 133 (2016).

[35] A. Qu, X. Xu, Y. Zhang, Y. Li, W. Zha, S. Wen, H. Xie, J. Wang, A nitrogen-rich mesoporous polymer for photocatalytic hydrogen evolution from water, React. Funct. Polym. 102 (2016) 93-100.

[36] X. He, W. Zhang, R. Yang, The characterization of DOPO/MMT nanocompound and its effect on flame retardancy of epoxy resin, Compos. Part A-Appl. S. 98 (2017) 124-135.

[37] P. Wang, Z. Cai, Highly efficient flame-retardant epoxy resin with a novel DOPO-based triazole compound: Thermal stability, flame retardancy and mechanism, Polym. Degrad. Stabi. 137 (2017) 138-150.

[38] C. Hu, T. Yu, Y. Li, Novel DOPO-Modified Graphene: Synthesis and Characterization, J. Nanosci. Nanotech. 17 (2017) 4894-4900.

[39] B. Yu, Y. Shi, B. Yuan, S. Qiu, W. Xing, W. Hu, L. Song, S. Lo, Y. Hu, Enhanced thermal and flame retardant properties of flame-retardant-wrapped graphene/epoxy resin nanocomposites, J. Mater. Chem. A 3 (2015) 8034-8044.

[40] D. Luo, G. Zhang, J. Liu, X. Sun, Evaluation criteria for reduced graphene oxide, J. Phys. Chem. C 115 (2011) 11327-11335.

[41] X. Mu, B. Yuan, W. Hu, S. Qiu, L. Song, Y. Hu, Flame retardant and

anti-dripping properties of polylactic acid/poly (bis (phenoxy) phosphazene)/expandable graphite composite and its flame retardant mechanism, RSC Adv. 5 (2015) 76068-76078.

[42] W. Guo, B. Yu, Y. Yuan, L. Song, Y. Hu, In situ preparation of reduced graphene oxide/DOPO-based phosphonamidate hybrids towards high-performance epoxy nanocomposites, Compos. Part B-Eng. 123 (2017) 154-164.

[43] X. Wang, Y. Hu, L. Song, W. Xing, H. Lu, P. Lv, G. Jie, Flame retardancy and thermal degradation mechanism of epoxy resin composites based on a DOPO substituted organophosphorus oligomer, Polymer 51 (2010) 2435-2445.

[44] U. Braun, A.I. Balabanovich, B. Schartel, U. Knoll, J. Artner, M. Ciesielski, M. Döring, R. Perez, J.K. Sandler, V. Altstädt, Influence of the oxidation state of phosphorus on the decomposition and fire behaviour of flame-retarded epoxy resin composites, Polymer 47 (2006) 8495-8508.

[45] J.Y. Kim, W.H. Lee, J.W. Suk, J.R. Potts, H. Chou, I.N. Kholmanov, R.D. Piner, J. Lee, D. Akinwande, R.S. Ruoff, Chlorination of reduced graphene oxide enhances the dielectric constant of reduced graphene oxide/polymer composites, Adv. Mater. 25 (2013) 2308-2313.

Table captions

Table 1 XPS data of COFs and DOPO-COFs nanosheets.

Table 2 TGA data of COFs, COFs nanosheeets, and DOPO-COFs nanosheets under nitrogen atmosphere.

Table 3 Cone calorimeter, LOI and UL-94 vertical burning tests data of EP and its nanocomposites.

Table 1 XPS data of COFs and DOPO-COFs nanosheets.

Sample	C (at%)	O (at%)	N (at%)	P (at%)
COFs nanosheets	64.9	7.6	27.5	-
FCOFs nanosheets	63.0	11.6	24.7	0.7

Table 2 TGA data of COFs, COFs nanosheeets, and DOPO-COFs nanosheets under nitrogen atmosphere.

Sample	$T_{5\ wt\%}$ (^oC)	T_{max} (^oC)	Residue (wt%)
COFs	334	416	26.9
NCOFs	199	353	32.6
DOPO-NCOFs	301	342	39.3

NCOFs: COFs nanosheets

Table 3 Cone calorimeter, LOI and UL-94 vertical burning tests data of EP and its nanocomposites.

Sample	TTI (s)	PHRR (kW/m^2)	THR (MJ/m^2)	LOI (%)	UL-94
EP 0	58.0	1369	135.6	23.5	NR
EP 1	70.2	1295	133.4	23.5	NR
EP 2	64.0	1086	125.3	24.0	NR
EP 3	58.6	1227	131.5	24.5	NR
EP 4	60.7	1117	110.5	25.0	NR
Control	55.0	1295	140.4	24	NR

NR：No rating.

Figure captions

Figure. 1 Schematic for (a) synthetic route of bulk COFs; (b) preparation process of DOPO-COFs nanosheets and EP nanocomposites.

Figure. 2 (a) FTIR spectra and of COFs, DOPO-COFs nanosheets, and DOPO; (b) XRD patterns of COFs and DOPO-COFs nanosheets; TEM image of (c) COFs, (d) DOPO-COFs nanosheets and (e) EDS pattern of DOPO-COFs nanosheets.

Figure. 3 (a) AFM image of DOPO-COFs nanosheets; (b) height profiles along the lines in image (a); (c) three-dimensional image of DOPO-COFs nanosheets in image (a).

Figure. 4 (a) wide XPS scanning spectrum of DOPO-COFs nanosheets; high-resolution (b) C_{1s}, (c) N_{1s}, and (d) P_{2p} XPS spectra of DOPO-COFs nanosheets.

Figure. 5 (a,b) TGA and DTG curves of COFs, COFs nanosheets and DOPO-COFs nanosheets under nitrogen atmosphere; (c,d) TGA and DTG curves of EP and its nanocomposites under nitrogen atmosphere.

Figure. 6 SEM images of fractured surface of (a,b) EP 0, (c,d) EP 4, and (e,f) EP Control at different magnifications.

Figure. 7 TEM ultrathin section images of (a) EP Control and (b) EP 4.

Figure. 8 (a) Storage modulus and (b) stress-strain curves of EP 0, EP 4, and EP Control.

Figure. 9 (a) HRR and (b) THR curves of EP and its nanocomposites.

Figure. 10 Digital images of (a) EP 0, (b) EP 1, (c) EP 2, (d) EP 3, (e) EP 4, and (f) EP Control after cone calorimetry tests.

Figure. 11 FTIR spectra of pyrolysis products from EP 0 and EP 4 at the maximum evolution rate.

Figure. 12 Absorbance of characteristic peaks of volatilized pyrolysis products of EP 0 and EP 4.

Figure. 13 Raman spectra of char residues of (a) EP 0, (b) EP 1, (c) EP 4, and (d) EP Control.

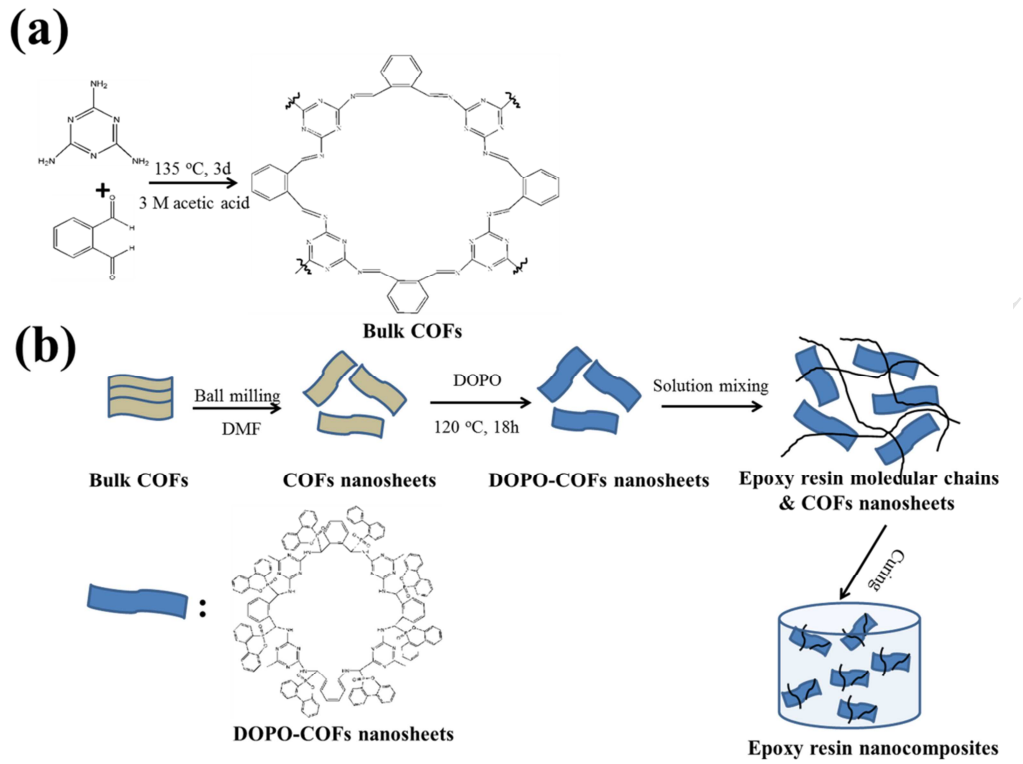

Figure. 1 Schematic for (a) synthetic route of bulk COFs; (b) preparation process of DOPO-COFs nanosheets and EP nanocomposites.

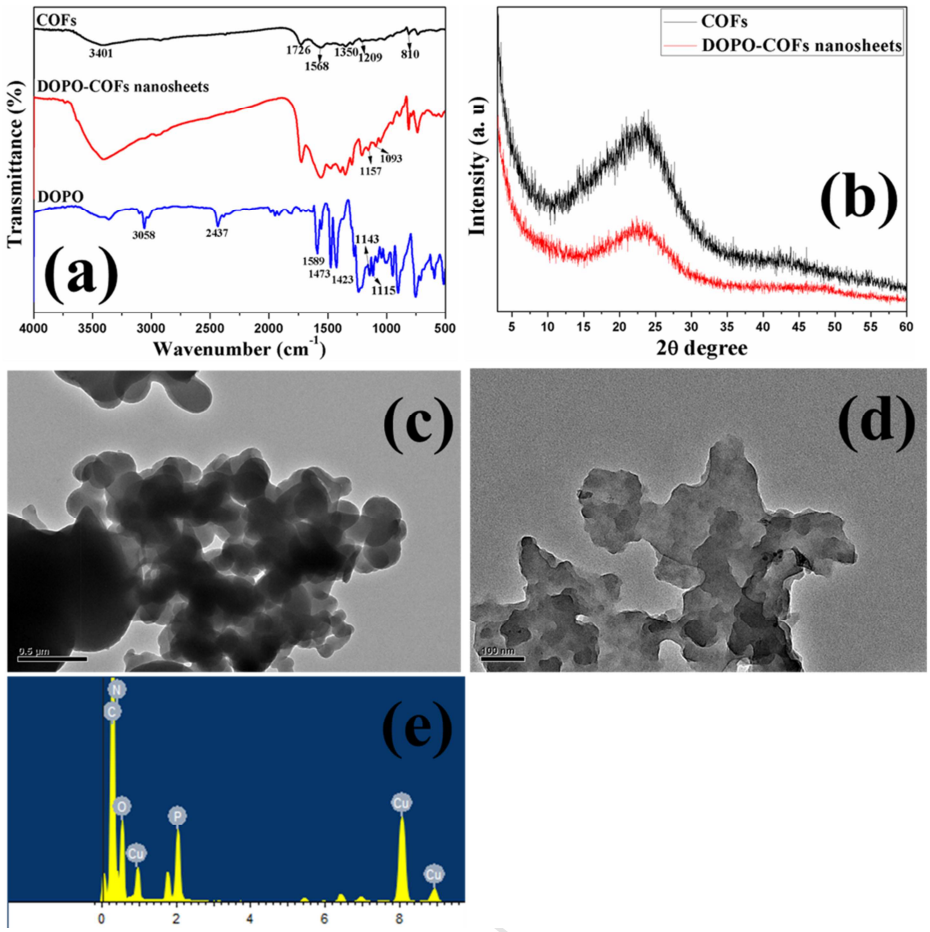

Figure. 2 (a) FTIR spectra and of COFs, DOPO-COFs nanosheets, and DOPO; (b) XRD patterns of COFs and DOPO-COFs nanosheets; TEM image of (c) COFs, (d) DOPO-COFs nanosheets and (e) EDS pattern of DOPO-COFs nanosheets.

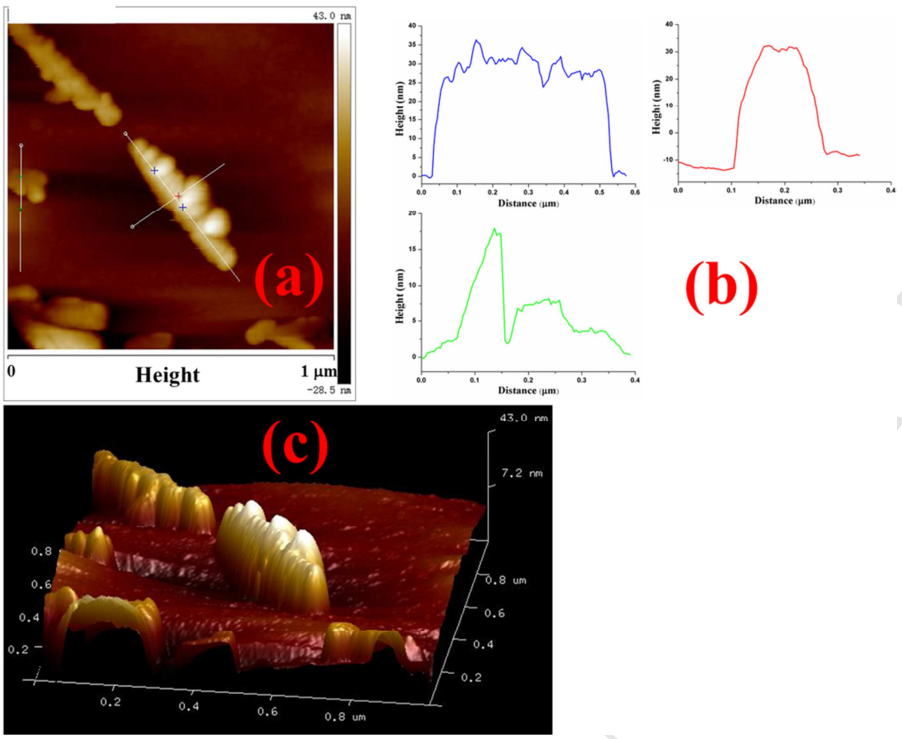

Figure. 3 (a) AFM image of DOPO-COFs nanosheets; (b) height profiles along the lines in image (a); (c) three-dimensional image of DOPO-COFs nanosheets in image (a).

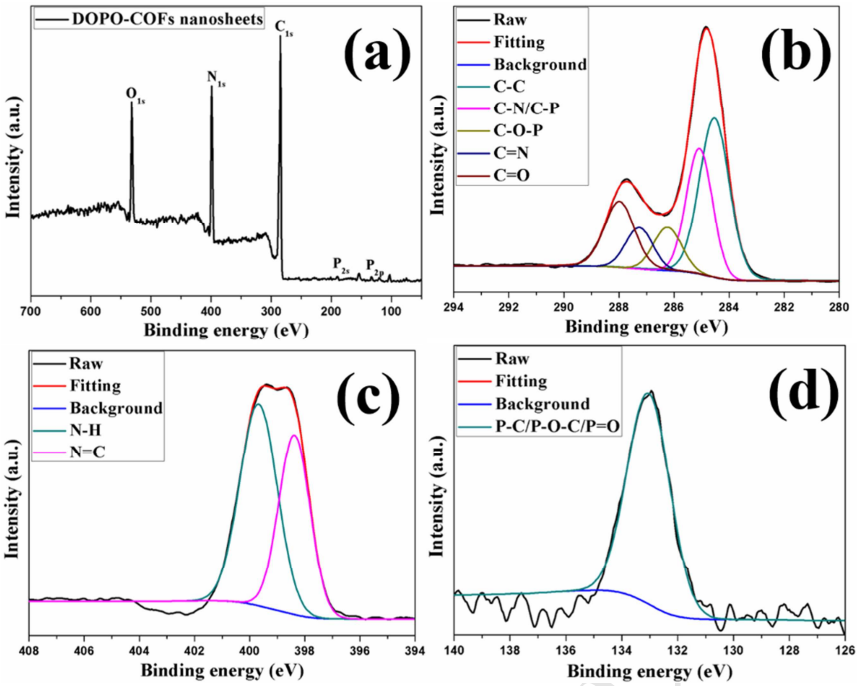

Figure. 4 (a) wide XPS scanning spectrum of DOPO-COFs nanosheets;

high-resolution (b) C_{1s}, (c) N_{1s}, and (d) P_{2p} XPS spectra of DOPO-COFs nanosheets.

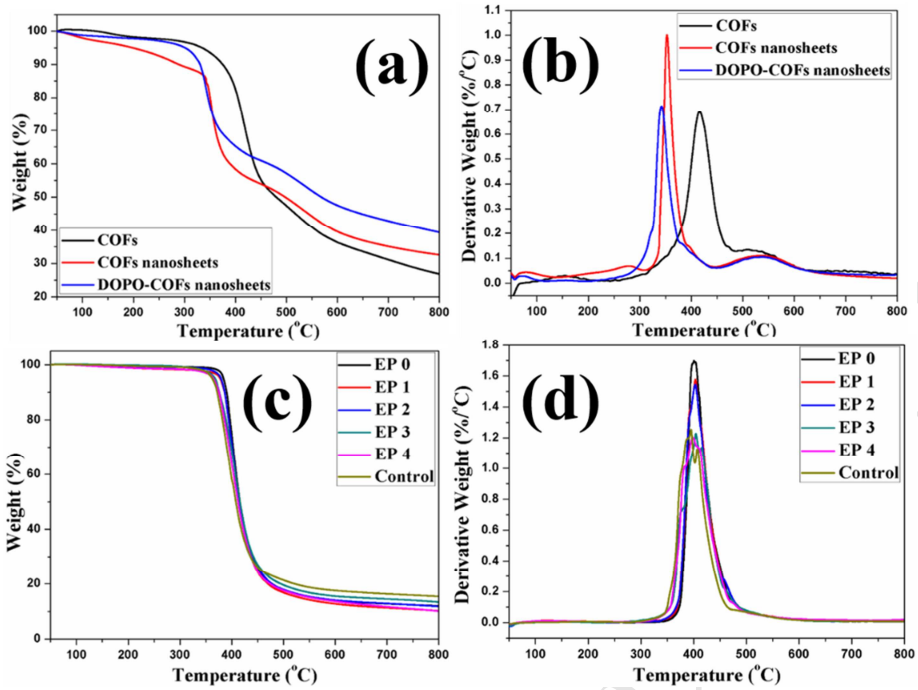

Figure. 5 (a,b) TGA and DTG curves of COFs, COFs nanosheets and DOPO-COFs nanosheets under nitrogen atmosphere; (c,d) TGA and DTG curves of EP and its nanocomposites under nitrogen atmosphere.

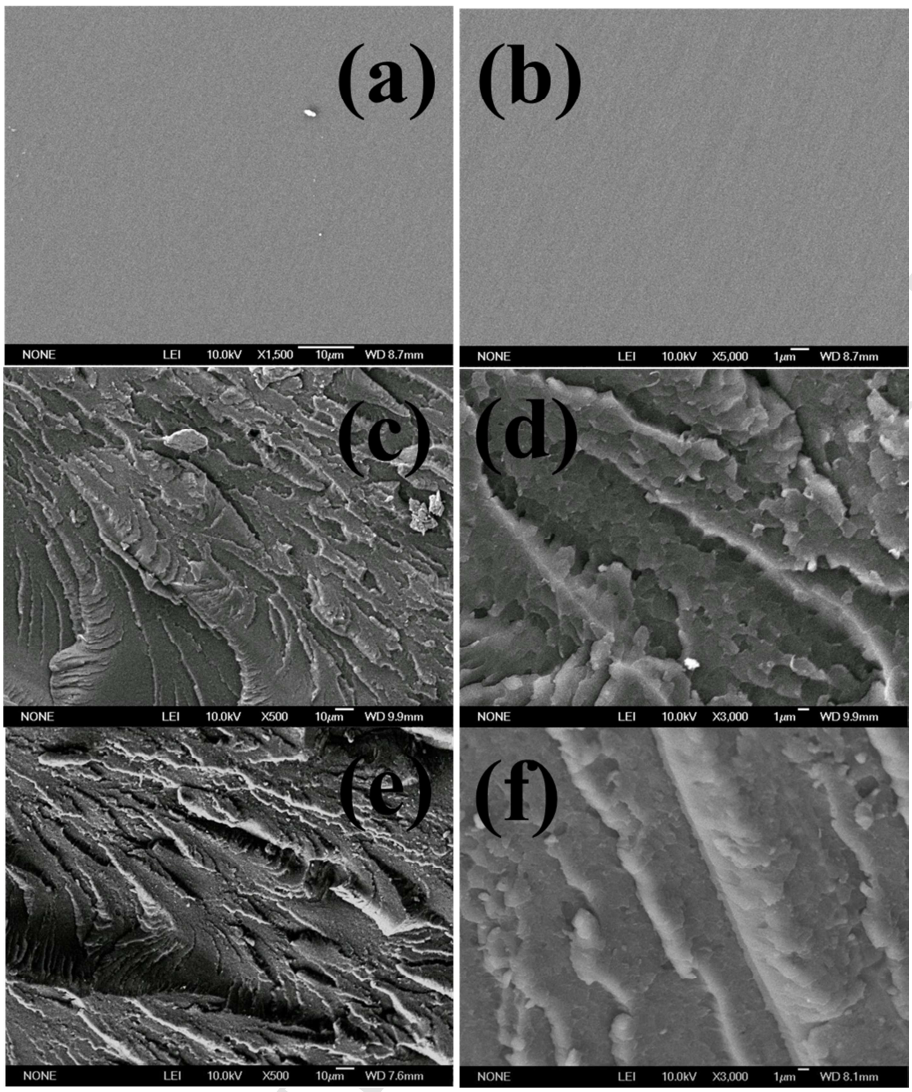

Figure. 6 SEM images of fractured surface of (a,b) EP 0, (c,d) EP 4, and (e,f) EP Control at different magnifications.

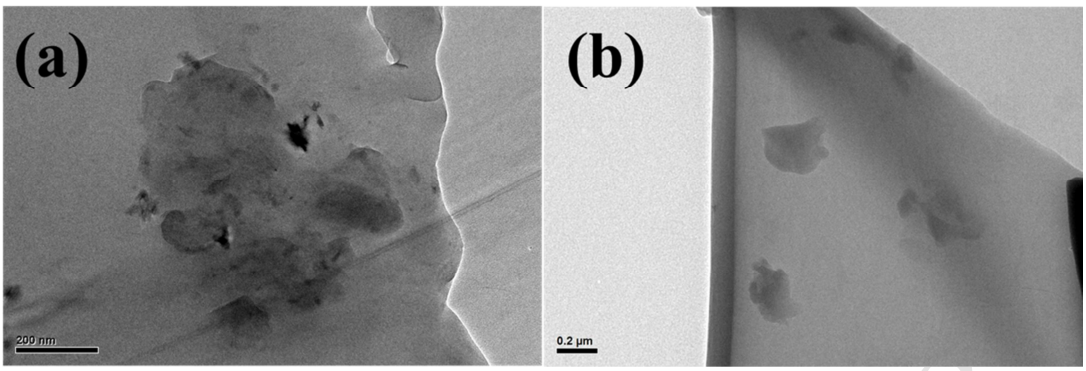

Figure. 7 TEM ultrathin section images of (a) EP Control and (b) EP 4.

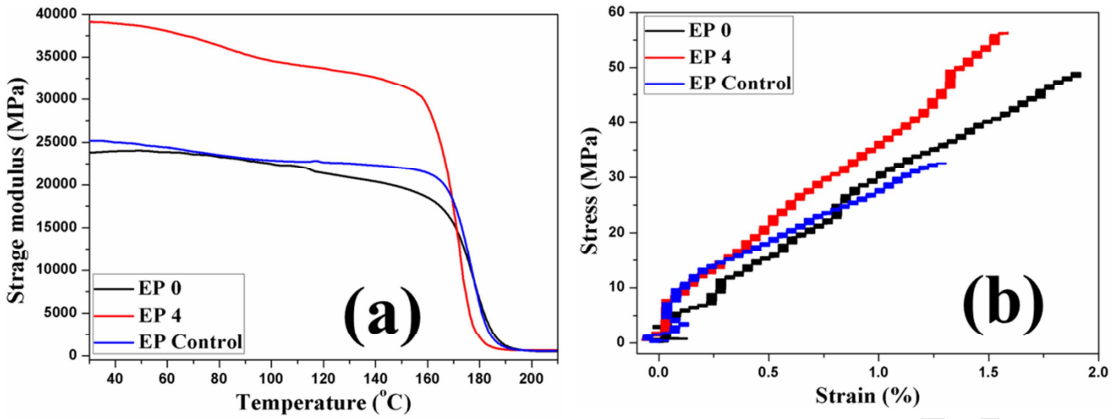

Figure. 8 (a) storage modulus and (b) stress-strain curves of EP 0, EP 4, and EP Control.

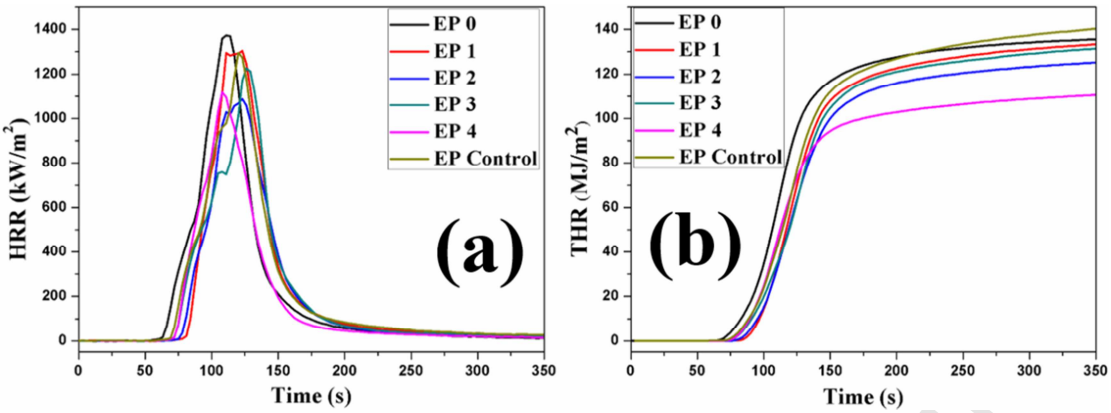

Figure. 9 (a) HRR and (b) THR curves of EP and its nanocomposites.

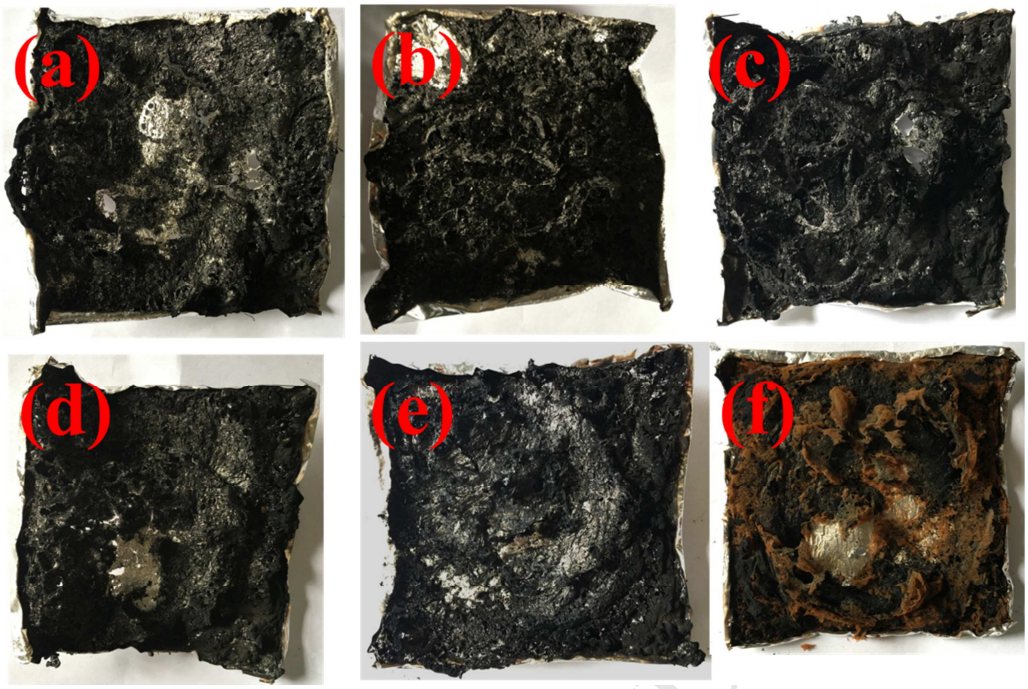

Figure. 10 Digital images of (a) EP 0, (b) EP 1, (c) EP 2, (d) EP 3, (e) EP 4, and (f) EP Control after cone calorimetry tests.

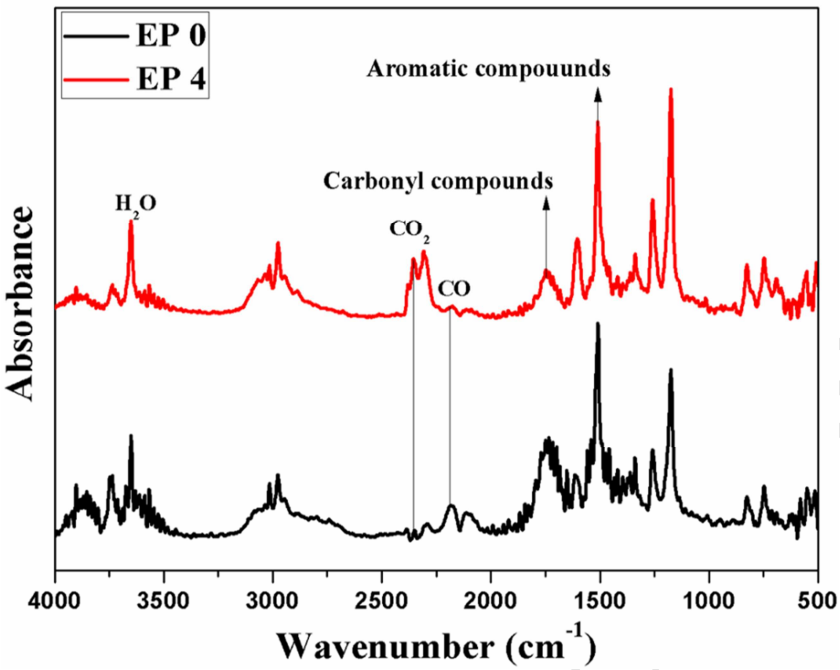

Figure. 11 FTIR spectra of pyrolysis products from EP 0 and EP 4 at the maximum evolution rate.

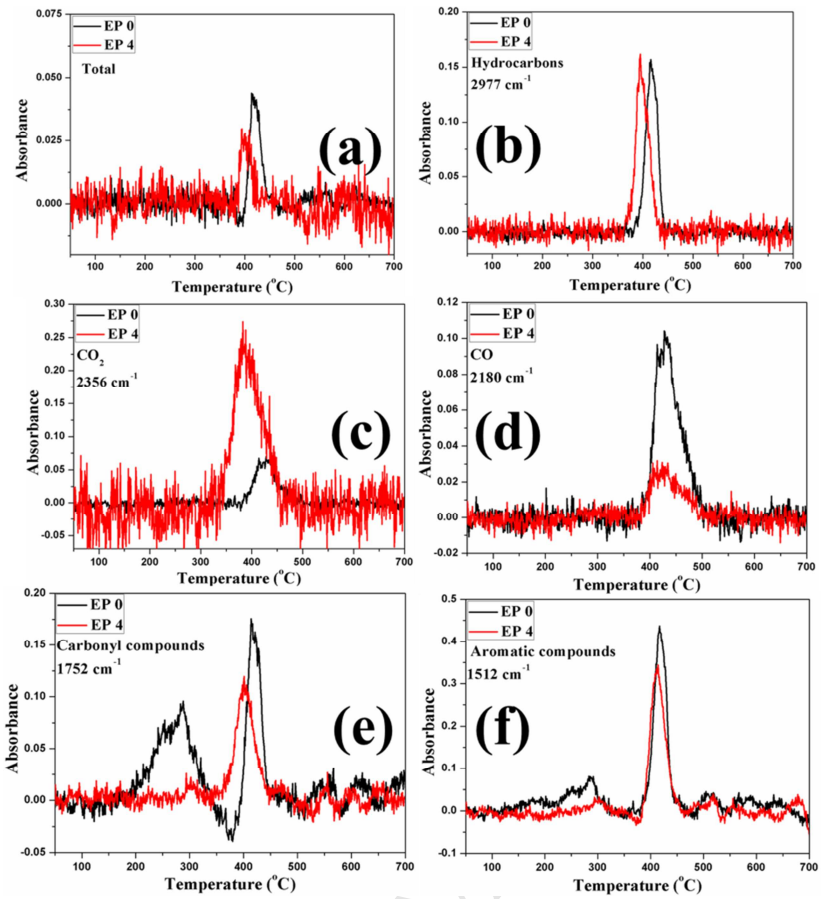

Figure. 12 Absorbance of characteristic peaks of volatilized pyrolysis products of EP 0 and EP 4.

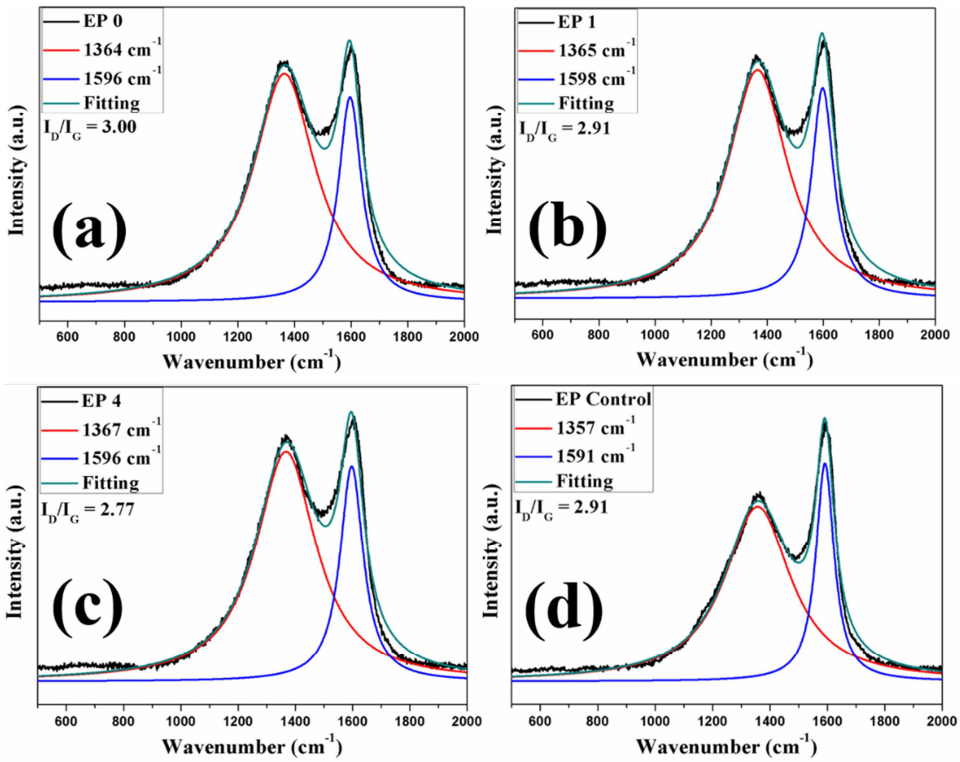

Figure. 13 Raman spectra of char residues of (a) EP 0, (b) EP 1, (c) EP 4, and (d) EP Control.

Highlights

A novel phosphorus and nitrogen containing covalent organic frameworks (DOPO -COFs) nanosheet has been synthesized first.

The dispersibility of DOPO-COFs nanosheets, the flame retardancy (PHRR, THR, thermal degradation rate, and char residues), mechanical performance and CO suppression of EP/DOPO-COFs nanosheets have been enhanced obviously.

The feasible mechanism for inhibiting fire hazard of EP nanocomposites has also been put forward.